

Robust Methods for Multiscale Coarse Approximations of Diffusion Models in Perforated Domains

Miranda Boutilier^{a,*}, Konstantin Brenner^{a,b}, Victorita Dolean^{a,c}

^a*Université Côte d'Azur, Laboratoire J.A. Dieudonné, CNRS UMR 7351, Nice, 06108, France*

^b*Team COFFEE, INRIA Centre at Université Côte d'Azur, Nice, 06108, France*

^c*University of Strathclyde, Department of Mathematics and Statistics, Glasgow, G1 1XH, U.K.*

Abstract

For the Poisson equation posed in a domain containing a large number of polygonal perforations, we propose a low-dimensional coarse approximation space based on a coarse polygonal partitioning of the domain. Similarly to other multiscale numerical methods, this coarse space is spanned by locally discrete harmonic basis functions. Along the subdomain boundaries, the basis functions are piecewise polynomial. The main contribution of this article is an error estimate regarding the H^1 -projection over the coarse space which depends only on the regularity of the solution over the edges of the coarse partitioning. For a specific edge refinement procedure, the error analysis establishes superconvergence of the method even if the true solution has a low general regularity. Combined with domain decomposition (DD) methods, the coarse space leads to an efficient two-level iterative linear solver which reaches the fine-scale finite element error in few iterations. It also bodes well as a preconditioner for Krylov methods and provides scalability with respect to the number of subdomains. Numerical experiments showcase the increased precision of the coarse approximation as well as the efficiency and scalability of the coarse space as a component of a DD algorithm.

Keywords:

Domain decomposition, iterative methods, coarse approximation, multiscale methods

*Corresponding Author

Email addresses: miranda.boutilier@univ-cotedazur.fr (Miranda Boutilier),
konstantin.brenner@univ-cotedazur.fr (Konstantin Brenner),
work@victoritadolean.com (Victorita Dolean)

1. Introduction and Model Problem

Numerical modeling of overland flows plays an increasingly important role in predicting, anticipating, and controlling floods. Anticipating these flood events can aid in the positioning of protective systems including dams, dikes, or rainwater drainage networks. One of the challenges of this numerical modeling of urban floods is that small structural features (buildings, walls, etc.) may significantly affect the water flow. In particular, the representation of the structural features in the numerical model impacts both the timing and extent of the flood [43, 44, 2].

Modern terrain survey techniques including photogrammetry and Laser Imaging, Detection, and Ranging (LIDAR) allow us to acquire high-resolution topographic data for urban areas. The data set used in this article has been provided by Métropole Nice Côte d’Azur (MNCA) and allows for an infra-metric description of the urban geometries [4]. From the hydraulic perspective, these structural features can be assumed to be essentially impervious, and therefore represented as perforations (holes) in the model domain.

In this article, we consider a linear diffusion model. Let D be an open simply connected polygonal domain in \mathbb{R}^2 . We denote by $(\Omega_{S,k})_k$ a finite family of perforations in D such that each $\Omega_{S,k}$ is an open connected polygonal subdomain of D . The perforations are mutually disjoint, that is $\overline{\Omega_{S,k}} \cap \overline{\Omega_{S,l}} = \emptyset$ for any $k \neq l$. We denote $\Omega_S = \bigcup_k \Omega_{S,k}$ and $\Omega = D \setminus \overline{\Omega_S}$, assuming that the family $(\Omega_{S,k})_k$ is such that Ω is connected. Note that the latter assumption implies that $\Omega_{S,k}$ are simply connected.

We are interested in the boundary value problem given by

$$\begin{cases} -\Delta u = f & \text{in } \Omega, \\ \frac{\partial u}{\partial \mathbf{n}} = 0 & \text{on } \partial\Omega \cap \partial\Omega_S, \\ u = 0 & \text{on } \partial\Omega \setminus \partial\Omega_S, \end{cases} \quad (1)$$

where \mathbf{n} is the outward normal to the boundary and $f \in L^2(\Omega)$.

Let us denote by $(\cdot, \cdot)_{L^2(\Omega)}$ and $(\cdot, \cdot)_{H^1(\Omega)}$ the standard L^2 and H^1 scalar products, that is,

$$(u, v)_{L^2(\Omega)} = \int_{\Omega} uv \, d\mathbf{x} \quad \text{and} \quad (u, v)_{H^1(\Omega)} = \int_{\Omega} \nabla u \cdot \nabla v \, d\mathbf{x}.$$

Setting

$$H_{\partial\Omega \setminus \partial\Omega_S}^1(\Omega) = \{u \in H^1(\Omega) \mid u|_{\partial\Omega \setminus \partial\Omega_S} = 0\}, \quad (2)$$

the weak solution of (1) satisfies the following variation formulation: Find $u \in H^1_{\partial\Omega \setminus \partial\Omega_S}(\Omega)$ such that

$$(u, v)_{H^1(\Omega)} = (f, v)_{L^2(\Omega)} \quad \text{for all} \quad v \in H^1_{\partial\Omega \setminus \partial\Omega_S}(\Omega). \quad (3)$$

In the context of urban flood modeling, u represents the flow potential (pressure head) and $(\Omega_{S,k})_k$ can be thought of as a family of impervious structures such as buildings, walls, or other similar structures. Although the linear model (1) is overly simplified to be directly used for urban flood assessment, the more general nonlinear elliptic or parabolic models are common in free surface flow simulations. Such models arise from Shallow Water equations either by neglecting the inertia terms [3] or within the context of semi-implicit Froude-robust time discretizations [15].

Depending on the geometrical complexity of the computational domain, the numerical resolution of (1) may become increasingly challenging. The typical model domain (see for example Figure 1) resulting from the realistic description of the urban environment will contain numerous perforations that are represented on different scales. In this contribution we investigate two numerical strategies that are capable of handling the multiscale features of the urban geometries. Both methods consider two “levels” of space discretization (see Figure 2 for a visual of both levels). The first level is based on a coarse polygonal partitioning of Ω , while the second one is associated with the fine-scale triangulation and is designed to resolve the small scale details of the model domain. The coarse partitioning is used to decompose the solution of the problem (1) into the sum of the locally harmonic component and local subdomain contributions, where the subdomain contributions can be efficiently computed in parallel. This splitting leads to a system that can be seen as a continuous version of the Schur complement problem. We then introduce a low-dimensional space, called here Trefftz or discrete Trefftz space, that serves to approximate the locally harmonic component of the solution. This coarse approximation space is built upon basis functions that satisfy the local Laplace problems (either exactly or via a finite element approximation) and have polynomial traces along the boundaries of the coarse partitioning. Both continuous and discrete variants of the coarse space are discussed.

The first contribution of this article concerns the ability of the Trefftz space to approximate the locally harmonic component of the solution (or the solution itself). We present an a priori estimate in the energy norm which, for a specific edge refinement procedure, results in superconvergence of the method regardless of the general regularity of the solution. This theoretical finding is confirmed by

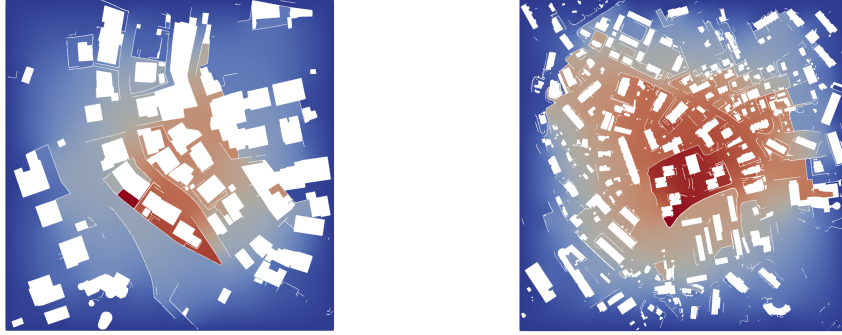


Figure 1: Finite element solution with $f = 1$ on model domains based on a smaller (left) and larger (right) data sets.

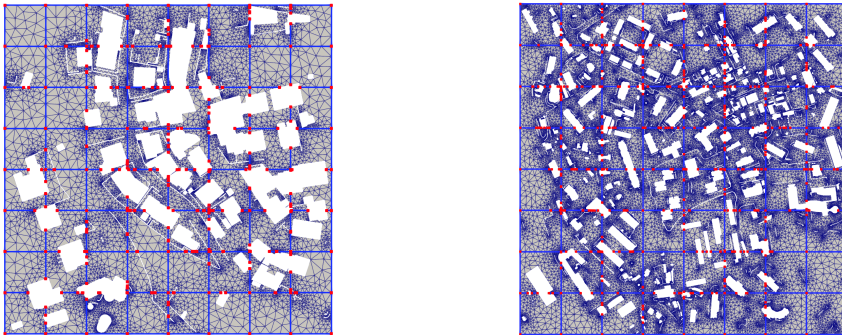


Figure 2: Coarse (thick lines) and fine (thin lines) discretizations for smaller (left) and larger (right) data sets, with the coarse nodes shown by red dots.

numerical experiments.

There exists an extensive literature on problems involving highly oscillatory coefficients or multiscale geometrical features, including for example the Localized Orthogonal Decomposition (LOD) method [31], heterogeneous multiscale methods (HMM) [41], or multiscale partition of unity methods such as the Generalized Finite Element Method (GFEM) [7] and the Multiscale Spectral Generalized Finite Element Method (Ms-GFEM) [8, 30]. In [8, 30], the optimal approximation spaces are constructed locally by solving generalized eigenvalue problems over a set of overlapping subdomains. The partition of unity functions are used to glue the local contributions into a globally conforming coarse approximation space. We note that these methods vary from the approach presented here as we consider nonoverlapping coarse cells and do not rely on eigenproblems.

Since the perforations in our model problem are structured, we can exploit the structural features of the heterogeneities. The method we consider here is closer to the Multiscale Hybrid-Mixed Method (MHM) [5], the Multiscale Finite Element Method (MsFEM) [27], or polytopal methods such as Virtual Element Methods (VEM) [13]. In MsFEM, the domain is partitioned into coarse cells, allowing the method to take advantage of parallel computing. Basis functions are then computed numerically based on the PDE on each coarse cell; in this way, our methodology is similar to MsFEM. In comparison to the classical MsFEM, our method leads to a larger coarse space. Compared to VEM, the major difference is that we numerically compute the approximation of the locally harmonic basis. By doing so, we manage to incorporate singular functions (corresponding to the corners of the domain) into the coarse space. We are also able to deal with very general polygonal cells (not star-shaped, not simply connected, etc.), which differs from VEM. Additionally, we willingly avoid using a method of fundamental solutions of any kind, because of our long-term motivation in problems more complex than the linear model problem (1). The MHM method combines ideas from the Mixed Finite Element Method (MFEM) and MsFEM. Compared to MHM, where Neumann traces are approximated by piecewise polynomials, our method is formulated in terms of approximate Dirichlet traces.

The second contribution of the article is the combination of the proposed coarse approximation with local subdomain solves in a two-level domain decomposition (DD) method. The idea of domain decomposition methods is to partition the domain into multiple subdomains and solve on each subdomain locally, gluing the local solutions together at the end to obtain a global solution. This results in an efficient iterative solver for the algebraic system resulting from the fine-scale finite element method. The obtained algorithm can also be thought as a way

of improving the precision of the original coarse approximation in the spirit of iterative multiscale methods (see e.g. [25]). We note that furthermore, the discrete Trefftz coarse space can also be combined with domain decomposition methods to provide a two-level preconditioner for Krylov methods. The coarse component provides robustness of the preconditioned Krylov method in terms of iteration counts with respect to the number of subdomains. It also provides an additional acceleration when compared to the iterative method. We refer the reader to two previous articles by the same authors [9, 10] while noting that this article serves as a completely summary of these papers with additional content and theory included.

Specifically on perforated domains with small and numerous perforations, the authors of [29] also introduced an enriched MsFEM-like method with Dirichlet boundary conditions on the holes, providing an error estimate as well. This method is extended with bubble functions in [16, 14]. The author of [39] also provide an MsFEM method for perforated domains, providing numerical results for domains with numerous small, regular perforations. As the model problem in [39] involves the Li-ion battery model, various boundary conditions (zero Neumann, nonlinear Neumann, etc.) are posed on the perforation boundaries (as is done here).

While literature on DD approaches to solve model problems in perforated domains is limited, the model problem can be thought of as the extreme limit case of the elliptic model containing highly contrasting coefficients with zero conductivity on the perforations. Two-level domain decomposition methods have been extensively studied for such heterogeneous problems. There are many classical results for coarse spaces that are constructed to resolve the jumps of the coefficients; see [20, 19, 32] for further details. Robust coarse spaces have constructed using the ideas from MsFEM in [1, 24]. Approaches to obtain a robust coarse space without careful partitioning of the subdomains include spectral coarse spaces such as those given in [22, 33, 18, 38]. The authors of [36] discuss these varied coefficient problems in the case where the coarse grid is not properly aligned with the heterogeneities. The combination of spectral and MsFEM methods can be found in [23], where the authors enrich the MsFEM coarse space with eigenfunctions along the edges. Additionally, the family of GDSW (Generalized Dryja, Smith, Widlund) methods [17] employ energy-minimizing coarse spaces and can be used to solve heterogeneous problems on less regular domains. These spaces are discrete in nature and involve both edge and nodal basis functions. To deal with coefficient jumps in highly heterogeneous problems, an adaptive GDSW coarse space was introduced in [26].

The article is laid out as follows. In Section 2, we introduce the continuous Trefftz coarse space and discuss its approximation properties. In Section 3, we

introduce the Trefftz coarse space in its discrete matrix form. With this, we provide the matrix forms of the coarse approximation and domain decomposition methods. The two-level domain decomposition methods are presented as both an iterative solver and a preconditioner for Krylov methods. In Section 4, we provide numerical results for the Trefftz space used as a coarse approximation, in an iterative Schwarz method, and as a preconditioner for Krylov methods. We provide numerical results for two different types model domains; the first domain is a simplified domain with one perforation at the corner, and the second type of model domain is a realistic urban domain with numerous perforations. Section 5 concludes with a summary and brief description of future work.

2. Continuous Trefftz Approximation

In this section, we introduce the splitting of (3), inspired by the Schur method, and propose the continuous finite-dimensional coarse space that can be used to efficiently approximate the locally harmonic component of the solution. We perform the error analysis of the coarse Galerkin approximation. In this regard, the main results are Proposition 2.1 and Theorem 2.1.

2.1. Coarse Mesh and Space Decomposition

We begin with a coarse discretization of Ω which involves a family of polygonal cells $(\Omega_j)_{j=1,\dots,N}$, the so-called coarse skeleton Γ , and the set of coarse grid nodes that will be referred to by \mathcal{V} . The construction is as follows. Consider a finite nonoverlapping polygonal partitioning of D denoted by $(D_j)_{j=1,\dots,N}$ and an induced nonoverlapping partitioning of Ω denoted by $(\Omega_j)_{j=1,\dots,N}$ such that $\Omega_j = D_j \cap \Omega$. We will refer to $(\Omega_j)_{j=1,\dots,N}$ as the coarse mesh over Ω . Additionally, we denote by Γ its skeleton, that is $\Gamma = \bigcup_{j=1,\dots,N} \partial\Omega_j \setminus \partial\Omega_S$.

We define $H_\Delta^1(\Omega)$ as a subspace of $H^1(\Omega)$ composed of piece-wise harmonic functions, weakly satisfying the homogeneous Neumann boundary conditions on $\partial\Omega \cap \partial\Omega_S$ such that

$$H_\Delta^1(\Omega) = \{ u \in H^1(\Omega) \mid (u|_{\Omega_j}, v)_{H^1(\Omega_j)} = 0 \text{ for all } v \in H_{\partial\Omega_j \setminus \partial\Omega_S}^1(\Omega_j) \}. \quad (4)$$

In other words, $H_\Delta^1(\Omega)$ can be defined as $u \in H^1(\Omega)$ such that for all subdomains Ω_j , the equations

$$\begin{cases} -\Delta u|_{\Omega_j} = 0 & \text{in } \Omega_j, \\ \frac{\partial u}{\partial \mathbf{n}} = 0 & \text{on } \partial\Omega_j \cap \partial\Omega_S. \end{cases} \quad (5)$$

are satisfied in a weak sense. We further define the space $H_\Gamma^1(\Omega)$ as the subspace of functions vanishing on the coarse skeleton Γ such that

$$H_\Gamma^1(\Omega) = \{ u \in H^1(\Omega) \mid u|_\Gamma = 0 \}. \quad (6)$$

By definition, $H_\Delta^1(\Omega)$ is orthogonal to $H_\Gamma^1(\Omega)$. Since $H_\Gamma^1(\Omega)$ is a closed subspace of $H^1(\Omega)$, we deduce that $H^1(\Omega) = H_\Delta^1(\Omega) \oplus H_\Gamma^1(\Omega)$ (see e.g. [35]). In other words, a given function $v \in H^1(\Omega)$ admits a unique decomposition into $v_\Delta + v_b$, where $v_\Delta \in H_\Delta^1(\Omega)$, $v_b \in H_\Gamma^1(\Omega)$ and $(v_\Delta, v_b)_{H^1(\Omega)} = 0$. Although for simplicity we will call v_Δ the “locally harmonic” or “piece-wise” harmonic component of v , we wish to stress that the space $H_\Delta^1(\Omega)$ also contains the information about the normal traces of v_Δ over $\partial\Omega_S$. The function v_b will be referred to as the local or “bubble” component of v .

Using the orthogonal decomposition of $H^1(\Omega)$ introduced above, we can express the weak formulation of (1) as the following Schur complement problem: Find $u = u_\Delta + u_b$ with $u_\Delta \in H_\Delta^1(\Omega) \cap H_{\partial\Omega \setminus \partial\Omega_S}^1(\Omega)$ and $u_b \in H_\Gamma^1(\Omega)$ satisfying

$$\begin{cases} (u_\Delta, v)_{H^1(\Omega)} = (f, v)_{L^2(\Omega)} & \forall v \in H_\Delta^1(\Omega) \cap H_{\partial\Omega \setminus \partial\Omega_S}^1(\Omega), \\ (u_b, v)_{H^1(\Omega)} = (f, v)_{L^2(\Omega)} & \forall v \in H_\Gamma^1(\Omega). \end{cases} \quad (7)$$

$$\quad (8)$$

We remark that the formulation (7)-(8) uncouples the local and the piece-wise harmonic components of u , moreover that the “bubble” component of the solution u_b can be computed from (8) locally (and in parallel) on each Ω_j , while the problem (7) remains globally coupled over the computational domain Ω .

2.2. Continuous Trefftz Space

We now proceed with the goal to approximate the locally harmonic component u_Δ of the solution. For this, we introduce the Trefftz coarse space, a finite-dimensional subspace of $H_\Delta^1(\Omega)$ that is spanned by functions that are piece-wise polynomial on the skeleton Γ .

Let $(e_k)_{k=1, \dots, N_e}$ denote a nonoverlapping partitioning of Γ such that each “coarse edge” e_k is an open planar segment, and we denote $H = \max_{k=1, \dots, N_e} |e_k|$. The set of coarse grid nodes is given by $\mathcal{V} = \bigcup_{k=1, \dots, N_e} \partial e_k$. Figure 3 illustrates the location of the nodal degrees of freedom that typically result from clipping $(D_j)_j$ with Ω_S . It is important to note that a straight segment of Γ may be subdivided into multiple edges. As we will show in Section 4, this subdivision can be intentional (see Figure 4) to achieve convergence of the coarse approximation.

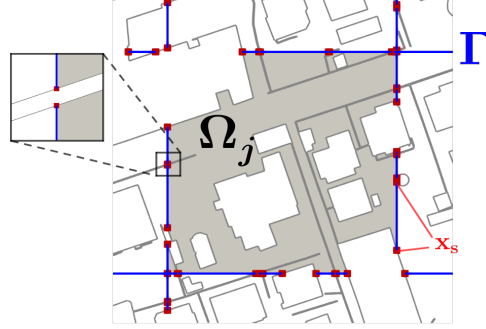


Figure 3: Coarse grid cell Ω_j , nonoverlapping skeleton Γ (blue lines), and coarse grid nodes $\mathbf{x}_s \in \mathcal{V}$ (red dots). Coarse grid nodes are located at $\bar{\Gamma} \cap \partial\Omega_S$.

We define

$$V_{H,p}^\Gamma = \{v \in C^0(\bar{\Gamma}) \mid v|_{e_k} \in \mathbb{P}_p(e_k) \text{ for all } k = 1, \dots, N_e\},$$

where $\mathbb{P}_p(e_k)$ denotes the set of polynomials of order (at most p) over an edge e .

We also define

$$V_{H,p} = \{v \in H_\Delta^1(\Omega) \mid v|_\Gamma \in V_{H,p}^\Gamma\}.$$

Let $(g_\alpha)_{\alpha=1,\dots,N_{H,p}}$ be some basis of $V_{H,p}^\Gamma$, where $N_{H,p}$ is the dimension of $V_{H,p}^\Gamma$. In practice, $(g_\alpha)_{\alpha=1,\dots,N_{H,p}}$ is set up by combining the set of the nodal piece-wise linear “hat” functions with the set of the higher order edge-based basis functions.

The function $\phi_\alpha \in V_{H,p}$ associated to g_α is computed by weakly imposing

$$\begin{cases} \Delta\phi_\alpha = 0 & \text{in } \Omega_j, \\ \frac{\partial\phi_\alpha}{\partial\mathbf{n}} = 0 & \text{on } \partial\Omega_j \cap \partial\Omega_S, \\ \phi_\alpha = g_\alpha & \text{on } \partial\Omega_j \setminus \partial\Omega_S. \end{cases} \quad (9)$$

The Galerkin method to approximate $u \in H_\Delta^1(\Omega)$ based on the coarse space reads as follows: find $u_H \in V_{H,p} \cap H_{\partial\Omega \setminus \partial\Omega_S}^1(\Omega)$ such that

$$(u_H, v)_{H^1(\Omega)} = (f, v)_{L^2(\Omega)} \quad \forall v \in V_{H,p} \cap H_{\partial\Omega \setminus \partial\Omega_S}^1(\Omega). \quad (10)$$

2.3. Error Analysis

We now provide an error estimate for the convergence of the Trefftz approximation space. We begin with few preliminary results that will be necessary in the proof.

Lemma 2.1 (Polynomial interpolation over an edge). *Let e_k be a coarse edge. We denote by \mathcal{I}_k^p the Lagrange interpolator of order p defined with respect to some set of interpolation points containing the endpoints of e_k . Then, there exists $c_0 = c_0(p) > 0$ such that for every v of sufficient regularity, we have*

$$\|v - \mathcal{I}_k^p v\|_{L^2(e_k)} + |e_k| \|v - \mathcal{I}_k^p v\|_{H^1(e_k)} \leq c_0 |e_k|^{p+1} |v|_{H^{p+1}(e_k)}.$$

This directly implies the following L^2 and H^1 estimates:

$$\|v - \mathcal{I}_k^p v\|_{L^2(e_k)} \leq c_0 H^{p+1} |v|_{H^{p+1}(e_k)} \quad \text{and} \quad \|v - \mathcal{I}_k^p v\|_{H^1(e_k)} \leq c_1 H^p |v|_{H^{p+1}(e_k)},$$

where $c_1 = c_0 (1 + H^2)^{1/2}$ can be bounded e.g. as $c_1 \leq c_0 (1 + \text{diam}(\Omega))^{1/2}$.

Proof. See Proposition 1.5 and 1.12 of [21]. See also Lemma 4.2 and Remark 4 of [40] for estimates with explicit dependency on p and higher dimension. \square

Lemma 2.2 (Gagliardo-Nirenberg interpolation inequality). *Let Ω be Lipschitz domain in \mathbb{R}^d and $\|\cdot\|_{s,q}$ denote the Slobodskii-Sobolev norm in $W^{s,q}(\Omega)$, $s \geq 0, q \geq 1$ (see the reference below). Let $s, s_1, s_2 \geq 0, 1 \leq q, q_1, q_2 \leq \infty$ and $\theta \in (0, 1)$ be such that*

$$s = \theta s_1 + (1 - \theta) s_2, \quad \frac{1}{r} = \frac{\theta}{q_1} + \frac{1 - \theta}{q_2}.$$

Then, there exists $c_{GN} = c_{GN}(s_1, q_1, s_2, q_2) > 0$ such that

$$\|u\|_{s,q} \leq c_{GN} \|u\|_{s_1,q_1}^\theta \|u\|_{s_2,q_2}^{1-\theta}$$

for all $u \in W^{s_1,q_1}(\Omega) \cap W^{s_2,q_2}(\Omega)$ as long as the following condition fails: s_2 is an integer ≥ 1 , $q_2 = 1$ and $s_2 - s_1 \leq 1 - 1/q_1$.

Proof. See Theorem 1 of [12] for details. \square

Corollary 2.1 (Interpolation in H^s). *Let $\|\cdot\|_s, s \geq 0$ denote the $H^s(\Omega) = W^{s,2}(\Omega)$ norm, where Ω satisfies the assumptions of Lemma 2.2. Let $0 \leq \theta \leq 1$ and $s = \theta s_1 + (1 - \theta) s_2$. There exists $c_{GN} = c_{GN}(s_1, s_2) > 0$ such that*

$$\|u\|_s \leq c_{GN} \|u\|_{s_1}^\theta \|u\|_{s_2}^{1-\theta},$$

for all $u \in H^{\max(s_1, s_2)}(\Omega)$.

Proof. The result follows from Lemma 2.2, setting $q_1 = q_2 = 2$ and using standard Sobolov embedding theory. \square

Lemma 2.3. *Let $1/2 < s \leq 1$ and let $g \in H^s(\partial\Omega_j \setminus \partial\Omega_S)$ satisfy $g|_{\partial(\Omega_j \cap \Gamma)} = 0$. Then, the function $\tilde{g} : \partial D_j \rightarrow \mathbb{R}$ defined by*

$$\tilde{g}(x) = \begin{cases} g(x) & x \in \partial(\Omega_j \cap \Gamma), \\ 0 & x \in \partial D_j \setminus \partial(\Omega_j \cap \Gamma) \end{cases}$$

belongs to $H^s(\partial D_j)$.

Proof. The proof is quite basic, for the full proof we refer e.g. to Lemma 5 of [11]. \square

Lemma 2.4. *Let $g \in H_0^1(\Gamma_j)$, then there exists $\phi \in H^1(\Omega_j)$ satisfying $\phi|_{\Gamma_j} = g$ such that*

$$|\phi|_{H^1(\Omega_j)} \leq c_{GN} C_j \|g\|_{L^2(\Gamma_j)}^{1/2} \|g\|_{H^1(\Gamma_j)}^{1/2},$$

where C_j only depends on D_j .

Proof. In view of Lemma 2.3, we can extend g on ∂D_j by zero so that the extension \tilde{g} is in $H^1(\partial D_j)$. Then, there exists $\tilde{\phi} \in H^1(\Omega_j)$ such that $\tilde{\phi} = \tilde{g}$ on ∂D_j and

$$|\tilde{\phi}|_{H^1(D_j)} \leq C_j \|\tilde{g}\|_{H^{1/2}(\partial D_j)}.$$

Using Sobolev interpolation, we have

$$\begin{aligned} |\tilde{\phi}|_{H^1(D_j)} &\leq c_{GN} C_j \|\tilde{g}\|_{L^2(\partial D_j)}^{1/2} \|\tilde{g}\|_{H^1(\partial D_j)}^{1/2} \\ &= c_{GN} C_j \|g\|_{L^2(\Gamma_j)}^{1/2} \|g\|_{H^1(\Gamma_j)}^{1/2}. \end{aligned}$$

The result follows by setting $\phi = \tilde{\phi}|_{\Omega_j}$. \square

With preliminary lemmas established, we present the following proposition that is a novel contribution of this article.

Proposition 2.1 (Interpolation error estimate). *Let $(\gamma_l)_{l=1,\dots,N_\gamma}$ be a finite nonoverlapping partitioning of Γ and v the element of $H_\Delta^1(\Omega)$ such that the traces of v belong to $H^{p+1}(\gamma_l)$ for all l and some $p = 1, 2, \dots$. Assume in addition that the set of coarse edges $(e_k)_k$ is a subdivision of $(\gamma_l)_l$. Then, there exists $\phi \in H^1(\Omega)$ such that $\phi|_\Gamma \in V_{H,p}^\Gamma$ and satisfying*

$$|v - \phi|_{H^1(\Omega)} \leq C H^{p+\frac{1}{2}} \left(\sum_{l=1}^{N_\gamma} |v|_{H^{p+1}(\gamma_l)}^2 \right)^{1/2}. \quad (11)$$

Proof. Since $u \in H^1(\gamma_l)$, it follows that $u \in C^0(\overline{\gamma_l})$. However, being in $H^{1/2}(\Gamma)$, u cannot have discontinuities. Therefore $u \in H^1(\Gamma)$ and thus is continuous on $\overline{\Gamma}$.

Let \mathcal{I}_Γ^p be an interpolation operator from $C^0(\Gamma)$ to $V_{H,p}^\Gamma$ such that $\mathcal{I}_\Gamma^p v|_{e_k} = \mathcal{I}_k^p v$ for all k , where \mathcal{I}_k^p is defined in Lemma 2.1. Let $E_\Gamma = u|_\Gamma - \mathcal{I}_\Gamma^p(v|_\Gamma)$, since, $E_\Gamma(x) = 0$ for every $x \in \mathcal{V}$, it follows from Lemma 2.4 that there exists $\psi_j \in H^1(\Omega_j)$ satisfying $\psi_j|_\Gamma = \widetilde{E}_\Gamma$ such that

$$|\psi_j|_{H^1(\Omega_j)} \leq c_{GN} C_j \|E_\Gamma\|_{L^2(\Gamma_j)}^{1/2} \|E_\Gamma\|_{H^1(\Gamma_j)}^{1/2}$$

Let $\phi \in H^1(\Omega)$ be defined as $\phi|_{\Omega_j} = u_\Delta|_{\Omega_j} - \psi_j|_{\Omega_j}$ for all Ω_j . We have

$$\begin{aligned} |v - \phi|_{H^1(\Omega_j)} &\leq c_{GN} C_j \|E_\Gamma\|_{L^2(\Gamma_j)}^{1/2} \|E_\Gamma\|_{H^1(\Gamma_j)}^{1/2} \\ &\leq c_{GN} C_j \left(\sum_l \|E_{\Gamma,j}\|_{L^2(\gamma_l \cap \Gamma_j)}^2 \right)^{1/4} \left(\sum_l \|E_{\Gamma,j}\|_{H^1(\gamma_l \cap \Gamma_j)}^2 \right)^{1/4} \end{aligned}$$

Since $(e_k)_k$ is a subdivision of $(\gamma_l)_l$, we deduce from Lemma 2.1

$$|v - \phi|_{H^1(\Omega_j)} \leq c_{GN} c_0 c_1 C_j H^{p+1/2} \left(\sum_l |u|_{H^{p+1}(\gamma_l \cap \Gamma_j)}^2 \right)^{1/2}. \quad (12)$$

By summing (12) over all Ω_j , we obtain (11) with $C = \sqrt{2} c_{GN} c_0 c_1 \max_j C_j$. \square

Proposition 2.2 (Best approximation). *The solution of (10) satisfies*

$$|u_\Delta - u_H|_{H^1(\Omega)} \leq |u_\Delta - \phi|_{H^1(\Omega)}$$

for any $\phi \in H^1(\Omega)$ such that $\phi|_\Gamma \in V_{H,p}^\Gamma$.

Proof. We first remark that, because u_H is the projection of u_Δ on $V_{H,p}$, it satisfies

$$|u_\Delta - u_H|_{H^1(\Omega)} \leq |u_\Delta - v_H|_{H^1(\Omega)} \quad (13)$$

for any $v_H \in V_{H,p}$. Given some $\phi \in H^1(\Omega)$ such that $\phi|_\Gamma \in V_{H,p}^\Gamma$, we set $v_H \in V_{H,p}^\Gamma$ be such that $v_H|_\Gamma = \phi|_\Gamma$. Since $u_\Delta - v_H \in H_\Delta^1(\Omega)$, we have that

$$|u_\Delta - v_H|_{H^1(\Omega)} \leq |u_\Delta - \phi|_{H^1(\Omega)}, \quad (14)$$

that is to say that $u_\Delta - v_H$ is the minimizer of $\psi \mapsto |\psi|_{H^1(\Omega)}$ over the set $\{\psi \in H^1(\Omega_j) \mid \psi = u_\Delta - v_H \text{ on } \Gamma_i\}$. The result follows by combining (13) and (14). \square

From the propositions 2.2 and 2.1, we deduce the following error estimate regarding the locally harmonic part of the solution.

Theorem 2.1. *Let u be a solution of (3) and u_Δ its H^1 projection on $H_\Delta^1(\Omega)$. Let u_H satisfy (10). Then, under the assumptions of Proposition 2.1 with u_Δ instead of v ,*

$$|u_\Delta - u_H|_{H^1(\Omega)} \leq CH^{p+\frac{1}{2}} \left(\sum_{l=1}^{N_\gamma} |u|_{H^{p+1}(\gamma_l)}^2 \right)^{1/2}.$$

Remark 2.1. *The coarse basis functions can be reused for various right-hand sides. However, if f changes, the local components satisfying (7) have to be recomputed. In order to avoid multiple solutions, one may wish to approximate the solution of (7) over a reduced basis. This can be achieved by precomputing bubble multiscale basis functions as in [42]. Alternatively, one may try to approximate u solely by u_H . In view of the orthogonality between $H_\Delta^1(\Omega)$ and $H_\Gamma^1(\Omega)$, we have*

$$|u - u_H|_{H^1(\Omega)}^2 = |u_\Delta - u_H|_{H^1(\Omega)}^2 + |u_b|_{H^1(\Omega)}^2.$$

While the first term in the right hand side can be estimated based on Theorem 2.1, the H^1 norm of u_b can be controlled using (8) and the local Poincaré inequalities. More precisely, we have

$$|u_b|_{H^1(\Omega_j)} \leq C_{P,j} \text{diam}(\Omega_j) \|f\|_{L^2(\Omega_j)}$$

where $C_{P,j}$ denote the Poincaré constants associated to Ω_j .

Remark 2.2. *The broken H^{k+1} norm in the right-hand side of (11) involves only the traces of the solution along the sections of the coarse skeleton. Therefore, this estimate is valid for u having low general regularity that is due, for example, to corner singularities. As a matter of fact, the estimate (11) provides an a priori criterion for the adaptation of the coarse mesh: one has to ensure that the edge norm in the right-hand side is small. For a sufficiently regular right-hand side f , this can be achieved by moving the coarse edges away from the “bad” perforation corners.*

We further note that Theorem 2.1 is especially valuable for a so-called space or edge refinement, which is a procedure that involves splitting the edges of an otherwise fixed coarse grid. In that case, one observes superconvergence of the error with a rate of $k + \frac{1}{2}$.

3. Discrete Trefftz Space and Two-level Schwarz Method

We begin with the algebraic formulation and implementation of the problem. Let us consider a triangulation \mathcal{T} of Ω which is assumed to be conforming with respect to the polygonal partitioning $(\Omega_j)_{j=1,\dots,N}$ (see Figure 2). We denote by $\mathcal{N}_{\overline{\Omega}}$ the set of the triangulation nodes. In order to account for Dirichlet boundary condition imposed on $\partial\Omega \setminus \partial\Omega_S$, we introduce a set of internal nodes

$$\mathcal{N}_{\Omega} = \{ \mathbf{x}_s \in \mathcal{N}_{\overline{\Omega}} \mid \mathbf{x}_s \notin \partial\Omega \setminus \partial\Omega_S \}.$$

The total number of nodes in \mathcal{N}_{Ω} is denoted by N_{Ω} .

We denote by V_h the space of functions that are continuous and triangle-wise polynomial on each triangle of \mathcal{T} , where h denotes the maximal element diameter, and by $V_{h,0}$ the space $V_h \cap H^1_{\partial\Omega \setminus \partial\Omega_S}(\Omega)$. The finite element method for the variational problem (3) consists in finding $u_h \in V_{h,0}(\Omega)$ such that

$$a(u_h, v_h) = (f, v_h) \quad \forall v_h \in V_{h,0}(\Omega). \quad (15)$$

Let us denote by $(\eta_s)_{s \in \mathcal{N}_{\overline{\Omega}}}$ the set of the standard finite element basis functions associated to the nodal degrees of freedom. The associated “fine-scale” finite element discretization results in the linear system

$$\mathbf{A}\mathbf{u} = \mathbf{f}, \quad (16)$$

where \mathbf{A} is a $N_{\Omega} \times N_{\Omega}$ matrix with elements

$$A_{ij} = a(\eta_{s_j}, \eta_{s_i}) = \int_{\Omega} \nabla \eta_{s_j} \cdot \nabla \eta_{s_i} \, d\mathbf{x},$$

and \mathbf{f} is the vector from $\mathbb{R}^{N_{\Omega}}$ with components $f_j = \int_{\Omega} f \eta_{s_j} \, d\mathbf{x}$.

Because the triangular mesh resolves the fine-scale structure of the domain, the system may be quite large and the size of the triangular elements may vary by several orders of magnitude. As a result, the matrix \mathbf{A} is expected to be poorly conditioned.

3.1. Discrete Trefftz Approximation

In most practical situations, the coarse basis functions defined by (9) can not be computed analytically. Therefore, we consider the finite element approximation of $V_{H,p}$. The basis of the discrete Trefftz space is obtained through the finite element

approximation of (9). The finite element discretization of (9) results in the system of the form

$$\tilde{\mathbf{A}}_j \boldsymbol{\phi}_s^j = \mathbf{b}_s^j,$$

where $\tilde{\mathbf{A}}_j$ is the local stiffness matrix and \mathbf{b}_s^j accounts for the Dirichlet boundary data in (9). Let $\bar{\mathbf{R}}_j$ denote the boolean restriction matrices corresponding to the nodes of $\bar{\Omega}_j$, and let $\boldsymbol{\phi}_s$ be a vector such that $\bar{\mathbf{R}}_j \boldsymbol{\phi}_s = \boldsymbol{\phi}_s^j$ for all $j = 1, \dots, N$. The discrete Trefftz space is then defined as the span of the basis functions $\boldsymbol{\phi}_s$, $s = 1, \dots, N_{H,p}$. Discretely, the coarse transition matrix \mathbf{R}_H is such that the k th row of \mathbf{R}_H is given by $\boldsymbol{\phi}_k^T$ for $k = 1, \dots, N_V$.

The finite element counterpart of (10) and therefore the discrete coarse approximation from Section 2.2 can be expressed algebraically as

$$\mathbf{u}_H = M_H^{-1} \mathbf{f}, \quad (17)$$

where

$$M_H^{-1} = \mathbf{R}_H^T (\mathbf{R}_H \mathbf{A} \mathbf{R}_H^T)^{-1} \mathbf{R}_H.$$

3.2. Discrete Two-level Schwarz Method

Now, we will show how the coarse approximation introduced in the previous section can be combined with the Restricted Additive Schwarz (RAS) method to construct a simple yet efficient iterative linear solver for the fine-scale finite element method.

Let $(\Omega'_j)_{j=1, \dots, N}$ denote the overlapping partitioning of Ω such that $\Omega_j \subset \Omega'_j$. In practice, each Ω'_j is constructed by propagating Ω_j by a few layers of triangles.

We denote by \mathbf{R}'_j the boolean restriction matrices corresponding to the nodes of Ω'_j and set $\mathbf{A}'_j = \mathbf{R}'_j \mathbf{A} (\mathbf{R}'_j)^T$. Here, the boolean matrices \mathbf{R}'_j are of size $(N_j \times N_\Omega)$, where N_j denotes the number of degrees of freedom in Ω'_j and N_Ω denotes the number of degrees of freedom in Ω .

Given this framework, we introduce the following iterative procedure. Generally, we take the coarse approximation as the initial iterate $\mathbf{u}^0 = \mathbf{u}_H$. This allows us to begin with the accuracy of the coarse approximation and continue to iterate to finite element precision. With this, the iteration is given by

$$\begin{aligned} \mathbf{u}^{n+\frac{1}{2}} &= \mathbf{u}^n + M_{RAS}^{-1} (\mathbf{f} - \mathbf{A} \mathbf{u}^n) \\ \mathbf{u}^{n+1} &= \mathbf{u}^{n+\frac{1}{2}} + M_H^{-1} (\mathbf{f} - \mathbf{A} \mathbf{u}^{n+\frac{1}{2}}) \end{aligned} \quad (18)$$

where

$$M_{RAS}^{-1} = \sum_{j=1}^N (\mathbf{R}'_j)^T \mathbf{D}_j (\mathbf{A}'_j)^{-1} \mathbf{R}'_j$$

and \mathbf{D}_j denote the partition-of-unity matrices satisfying

$$I_N = \sum_{j=1}^N (\mathbf{R}'_j)^T \mathbf{D}_j (\mathbf{R}'_j),$$

where I_N is the identity matrix of size $(N_\Omega \times N_\Omega)$.

Additionally, we introduce the preconditioned system

$$M_{RAS,2}^{-1} \mathbf{A} \mathbf{u} = M_{RAS,2}^{-1} \mathbf{f}, \quad (19)$$

where the two-level discrete Restricted Additive Schwarz preconditioner is given additively by

$$M_{RAS,2}^{-1} = \mathbf{R}_H^T (\mathbf{R}_H \mathbf{A} \mathbf{R}_H^T)^{-1} \mathbf{R}_H + \sum_{j=1}^N (\mathbf{R}'_j)^T \mathbf{D}_j (\mathbf{A}'_j)^{-1} \mathbf{R}'_j.$$

We expect the use of a well-constructed preconditioner to provide acceleration in terms of Krylov iteration count. Generally, using preconditioned Krylov methods produces faster convergence than the iterative solver, both in terms of computation time and iterations.

We note that iteration (18) can be written as

$$\mathbf{u}^{n+1} = \mathbf{u}^n + (M_H^{-1} + M_{RAS}^{-1} (\mathbf{I} - \mathbf{A} M_H^{-1})) (\mathbf{f} - \mathbf{A} \mathbf{u}^n), \quad (20)$$

a hybrid method. We implement this hybrid iterative method as an additive method will not converge and a hybrid method is necessary for convergence. However, we choose to use the additive two-level RAS preconditioner (19) for Krylov methods as it is commonly used in domain decomposition literature and has an increased capacity for parallel computing. With this, we remark that we could use a hybrid method as a Krylov accelerator and that the Schwarz preconditioners presented here are not exhaustive.

In the context of domain decomposition, our coarse approximation is referred to as a “coarse space” for the Schwarz methods. However, we remark that the construction of the matrix form of the coarse approximation and coarse space are identical, with the difference being solely in application.

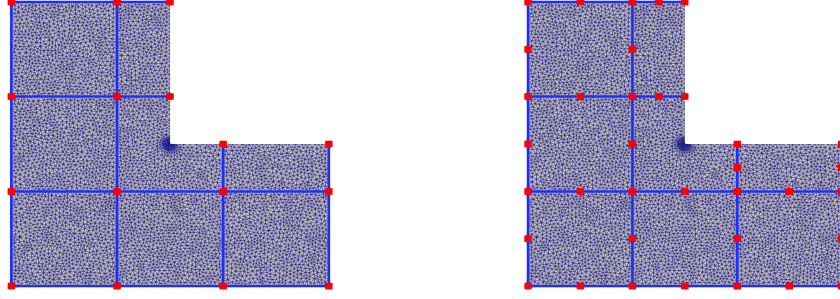


Figure 4: Coarse and fine discretizations of the L-shaped domain with 0 (left) and 1 (right) additional degree(s) of edge refinement.

4. Numerical Results

In this section, we illustrate the performance of the discrete Trefftz space in three different scenarios involving either a standalone Galerkin approximation (10), an iterative approach (18), or a preconditioner approach (19).

4.1. Coarse Approximation on L-Shaped Domain

To properly display the approximation properties, it is helpful to have an exact solution to the equation. However, the generation of this exact solution is difficult with multiple singularities. To combat this issue, we can use a model domain with one singularity/corner in the domain; an example of this would be an L-shaped domain with a reentering corner (Figure 4). The domain is defined by $D = (-1, 1)^2$, $\Omega_S = (0, 1)^2$ and $\Omega = D \setminus \overline{\Omega_S}$. We consider the problem (1) with zero right-hand side and a non-homogeneous Dirichlet boundary condition on $\partial\Omega \setminus \partial\Omega_S$ provided by the singular exact solution $u(r, \theta) = r^{\frac{2}{3}} \cos(\frac{2}{3}(\theta - \pi/2))$.

In order to assess the convergence of the discrete Trefftz method, we consider two strategies regarding the refinement of the coarse partitioning. The procedure involving the reduction of the diameter of the coarse cells will be referred to as *mesh refinement*. The sequence of such meshes will be constructed as follows: first the background domain D is partitioned into $N = (2k + 1)^2$, $k \in \mathbb{N}$, squares, then the coarse cells Ω_j are generated by excluding Ω_S . The choice of N being a square of an odd number ensures the consistency of the mesh sequence in terms of the shape of the elements. The second considered refinement strategy will be referred to as *edge refinement* procedure, which involves subdividing the edges of an original “ 3×3 grid”. This edge refinement approach is illustrated by Figure 4 and is inspired by the Multiscale Hybrid-Mixed method [5]. We remark that with

Ref. lvl.	H^1 semi-norm				L^2 norm			
	$p = 1$	eoc	$p = 2$	eoc	$p = 1$	eoc	$p = 2$	eoc
0	-1.098	-	-1.812	-	-1.881	-	-2.864	-
1	-1.601	1.669	-2.665	2.833	-2.762	2.925	-4.026	3.858
2	-2.132	1.765	-3.35	2.274	-3.677	3.042	-4.993	3.215
3	-2.626	1.641	-4.043	2.305	-4.514	2.781	-6.014	3.389

Table 1: Relative error and the experimental order of convergence for the Trefftz approximation with $p = 1, 2$ and using the edge refinement. Ref. level refers to the degree of additional edge refinement. Eoc refers to error of convergence.

both refinement procedures, it is ensured that none of the coarse grids will have degree of freedom located at the corner $(0, 0)$. As a result, the corner singularity will be captured by the basis functions associated with the L-shaped domain. We also note that in order to improve the precision of the fine-scale finite element method, the size of the triangles is graded in the vicinity of the corner $(0, 0)$.

Figure 5 reports, for both mesh and edge refinement strategies, the relative error in H^1 semi-norm and L^2 norm as functions of maximal coarse edge length H . The black dashed line represents the typical fine-scale finite element error; here, we use \mathbb{P}_2 finite elements. The relative error and the experimental order of convergence for edge refinement procedure are equally reported in Table 1. In accordance with the error estimate (11), for the edge refinement procedure, we observe superconvergence in the energy norm with rates of approximately $3/2$ and $5/2$ for $p = 1$ and $p = 2$, respectively. In the L^2 norm, the observed convergence rates are approximately 3 and $7/2$ for $p = 1$ and $p = 2$, respectively. In contrast to the edge refinement convergence, the convergence resulting from the mesh refinement seems to be controlled by the low global regularity of the solution. We observe the convergence rates typical for finite element methods on quasi-uniform meshes, that is, close to $2/3$ and $4/3$ in H^1 and L^2 norms, respectively.

4.2. Iterative DD and Preconditioned Krylov methods on L-Shaped Domain

We report on Figure 6 the convergence history of the iterative methods for the L-shaped domain. More precisely, we report two different error metrics, referred to as algebraic error and full error. For a given iterate, algebraic error is defined as a distance (based on L^2 or H^1 norms) between a given iterate and the solution of the algebraic system (16), while full error reflects the distance to the exact solution of (1). Figure 6 reports the convergence histories for linear systems resulting from an

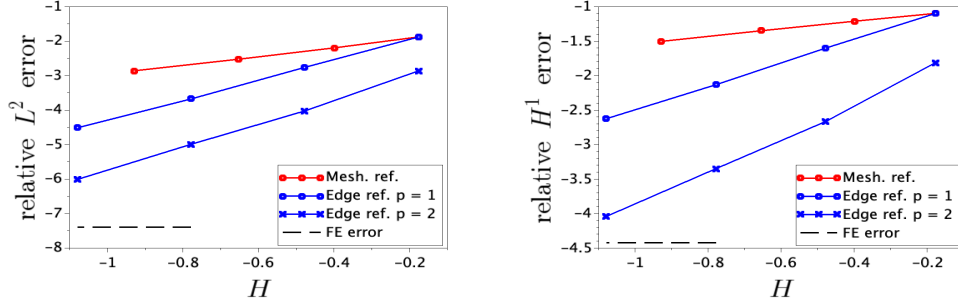


Figure 5: Coarse approximation error for L-shaped domain with edge (blue) and mesh (red) refinement in L^2 norm (left) and the energy norm (right). The black dashed line denotes the finite element error.

increasingly accurate background finite element discretization. We set the overlap to $\text{diam}(\Omega_j)/20$ and consider Trefftz spaces of order $p = 1$ and $p = 2$.

Because the width of the overlap is maintained constant, we observe on Figure 6 that the convergence of the iterative methods is not sensitive to the accuracy of the background finite element method until the precision of the latter is reached. The convergence of the preconditioned GMRES method is exponential, while the convergence curve of the algebraic error of the two-level fixed point method (18) exhibit two distinct slopes, with fast convergence at the initial stage. We note that the performance of both the stationary iteration and the preconditioned GMRES algorithm is improved when employing the higher order Trefftz space. We note that the initial slope of the stationary iteration method is approaching the slope of the preconditioned GMRES as the Trefftz order increases. In general, the results obtained in terms of the full error (right column of Figure 6) seem to point toward a following conclusion: the stationary iteration method appears to be an acceptable alternative to the preconditioned GMRES if very high accuracy is not required.

We further study the impact of edge refinement on the performance of the iterative methods. We report on Figure 7 the convergence of algebraic error in H^1 and L^2 norms for edge refinement up to degree three. This is reported for both the iterative and preconditioner approaches. We observe that reducing H not only improves the initial coarse approximation (the first iteration point), but also accelerates the convergence of the iterative methods. The most notable is the impact on the initial slope of the two-level iterative RAS method. Here, again, the initial slope of the stationary iteration method comes close to that of the preconditioned GMRES as we increase the order of edge refinement.

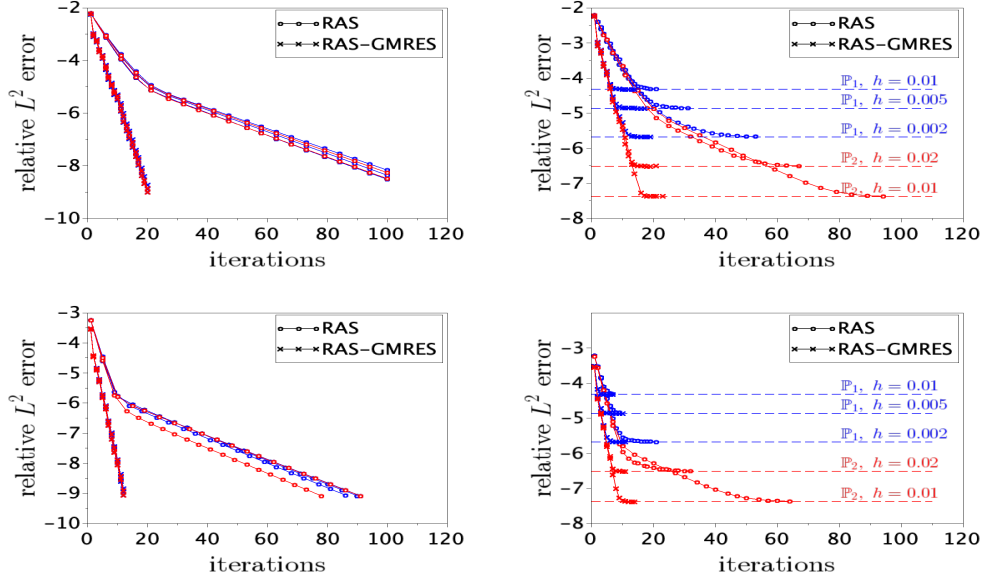


Figure 6: Convergence in L^2 of the two-level iterative (RAS) and preconditioned GMRES (RAS-GMRES) methods for the L-shaped domain on 5×5 subdomains with overlap of $\frac{1}{20}H$ and using first (top row) and second (bottom row) order Trefftz approximation. The dashed horizontal lines show the error of the fine-scale finite element method. Left to right: algebraic error, full error. Results for finite elements of order 1 and 2 are shown in blue and red, respectively.

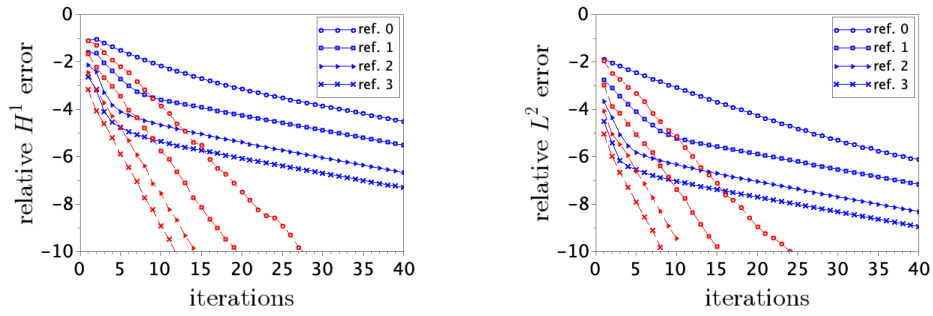


Figure 7: Convergence in H^1 (left) and L^2 (right) norms of the two-level iterative (blue) and preconditioned GMRES (red) methods for the L-shaped domain on 3×3 subdomains with overlap of $\frac{1}{20} \max_j \text{diam}(\Omega_j)$. Algebraic errors are shown for the first order Trefftz space with various degrees of edge refinement.

4.3. Iterative DD and Preconditioned Krylov Methods on Small Urban Domain

We examine the performance of the two-level stationary iteration and preconditioned GMRES methods over a domain based on realistic urban geometries for which the data sets were kindly provided by Métropole Nice Côte d’Azur. We focus here on a relatively small spatial frame shown on the left of Figure 1). The data frame is 160×160 meters and contains two kinds of structural features representing buildings (and assimilated small elevated structures) and walls in urban data. The number of perforations associated to building and wall is 63 and 77 respectively.. The triangulation of the domain is performed using Triangle [37]. This “small” model domain would take a minimum of 23 000 elements to triangulate without imposing maximum triangle area or constraining the mesh to match the coarse partitioning. Due to the geometric complexity of the computational domain, the mesh includes a number of very small triangles; the minimal triangle area is given as 5.83×10^{-13} . We consider the model problem (1) with $f = 1$, which we discretize with continuous piece-wise affine finite elements; the finite element solution is reported on the left of Figure 1.

We report on Figures 8 and 9 the convergence history of the stationary iterative method for different sizes of overlap. This figure shows results for both algebraic and full errors for various fine-scale discretization sizes h . The performance of the preconditioned GMRES is reported on Figures 10 and 11. In lieu of a true solution (which would exhibit multiple singularities), we provide a fine grid numerical solution to which the iterates are compared. The grid for the reference solution is generated via multiple levels of edge bisection (“red refinement”). We note that in contrast to the previous numerical experiment, we do not perform any mesh grading near the reentering corners of the domain; as a result, the finite element error is high.

We expose on Figure 8 the convergence history of the two-level stationary iteration method with overlap $\frac{1}{20}H$. We observe that the convergence of the algebraic error is robust with respect to h and that the fine-scale finite element method (black lines) can be reached in few steps. Further iterations do not improve the overall precision of the approximate solution even though the algebraic error may decrease. A stopping criteria which prevents excess iterations is warranted; such a posteriori estimates are discussed for example in [6, 28]. As expected, the performance of the stationary iteration method considerably deteriorates (see Figure 9) in the case of minimal geometric overlap.

Figures 10 and 11 report the performance of the two-level preconditioned GMRES method for overlaps of $\frac{1}{20}H$ and minimal geometric overlap, respectively. Compared to the stationary iterative method, major improvement is achieved for

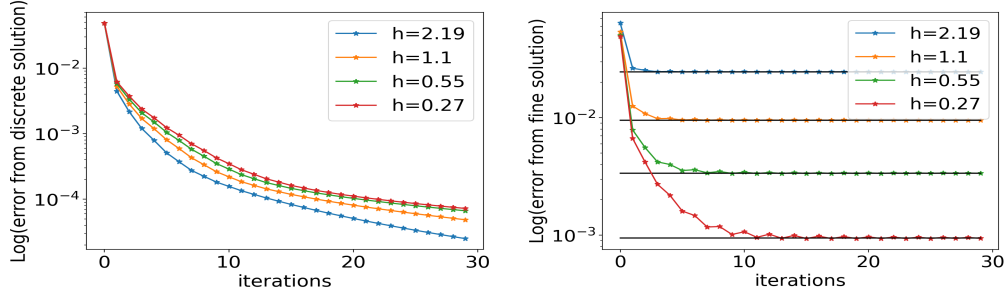


Figure 8: Convergence of the two-level iterative method for the urban data set on 8×8 subdomains with overlap $\frac{1}{20}H$. The black horizontal lines show the error of the fine-scale finite element method. Left to right: algebraic error, full error.

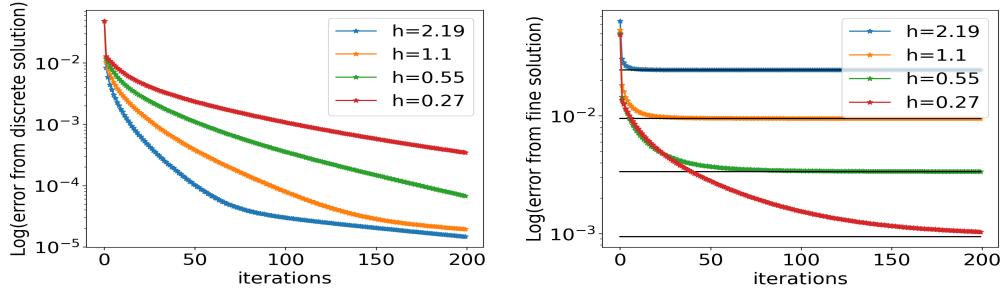


Figure 9: Convergence of the two-level iterative method for the urban data set on 8×8 subdomains with minimal geometric overlap. The black horizontal lines show the error of the fine-scale finite element method. Left to right: algebraic error, full error.

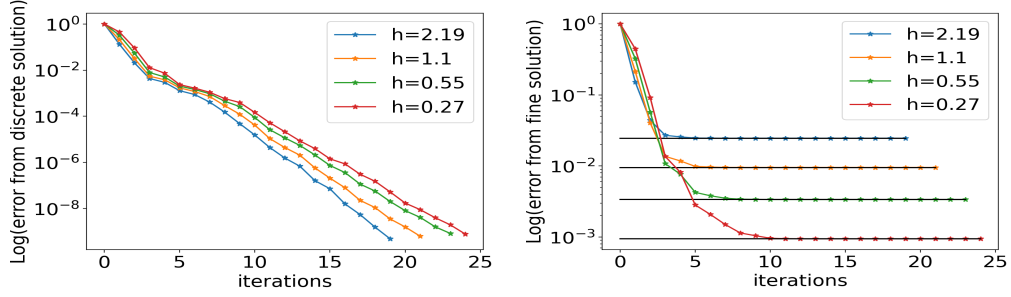


Figure 10: Convergence of the two-level preconditioned Krylov method for the urban data set on 8×8 subdomains with overlap $\frac{1}{20}H$. The black horizontal lines show the error of the fine-scale finite element method. Left to right: algebraic error, full error.

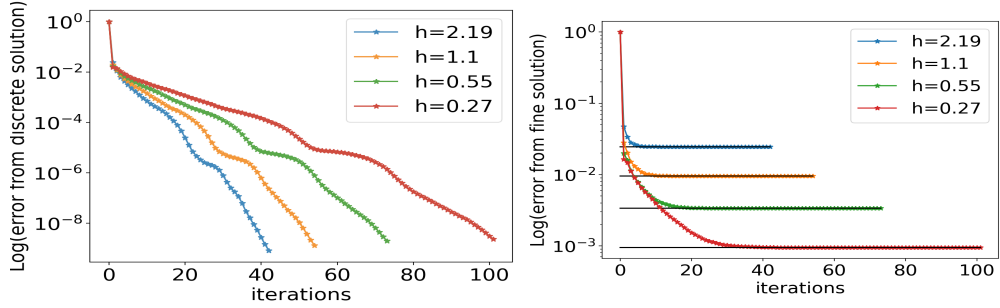


Figure 11: Convergence of the two-level preconditioned Krylov method for the urban data set on 8×8 subdomains with minimal geometric overlap. The black horizontal lines show the error of the fine-scale finite element method. Left to right: algebraic error, full error.

the case of minimal geometric overlap. However, due to low accuracy of the background finite element discretization, both the iterative and preconditioned GMRES methods perform comparably for the overlap of $\frac{1}{20}H$.

4.4. Scalability Tests for Preconditioned Krylov Method on Larger Urban Domain

As a final numerical experiment, we follow the experiment from the previous subsection and report the performance of the two-level preconditioned GMRES method on a larger data set shown on the right of Figure 1. This larger data set contains 306 buildings and 477 walls of varying sizes, the dimensions of the domain are 640×640 metres. The “large” model domain would take a minimum of 142 700 elements to triangulate without imposing maximum triangle area or constraining the mesh to match the coarse partitioning. The the minimal triangle area is observed to be 5.83×10^{-13} .

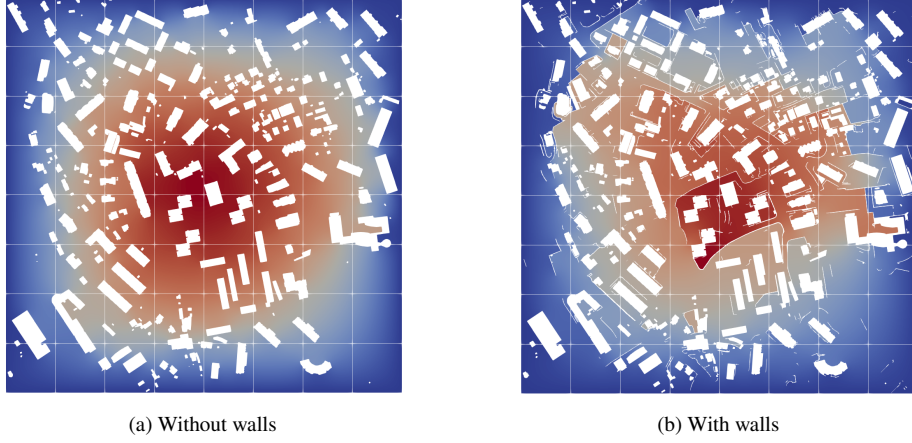


Figure 12: Approximate finite element solution over a computational domain divided in $N = 8 \times 8$ nonoverlapping subdomains.

We note that, depending on the partitioning of the domain, the perforations resulting from this data set (especially the wall data) can span across multiple coarse cells, which is a challenging situation for traditional coarse spaces. To further explore this observation, we will provide numerical results for data sets that do and do not include walls as perforations. Figure 12 reports the finite element solution obtained for a data set excluding and including walls. We can see from Figure 12 that the inclusion of walls noticeably affects the numerical solution.

For the sake of comparison, we also provide numerical results for the well-known Nicolaides coarse space [34], made of flat-top partition of unity functions associated with the overlapping partitioning. For the Nicolaides coarse space, scalability with respect to the number of subdomains is only guaranteed if the subdomains are connected. Therefore, to generate connected subdomains, we further partition $(\Omega'_j)_j$ into a family of connected subdomains. In other words, let m_j denote the number of disconnected components for each overlapping subdomain Ω'_j and let $\Omega'_{j,l}, l = 1, \dots, m_j$ denote the corresponding disconnected component. Then our new overlapping partitioning contains $m = \sum_{j=1}^N m_j$ total subdomains and is given by

$$(\widehat{\Omega}_k)_{k \in \{1, \dots, m\}} = ((\Omega'_{j,l})_{l \in \{1, \dots, m_j\}})_{j \in \{1, \dots, N\}}.$$

This special partitioning is visualized in Figure 13.

Then, the Nicolaides coarse space is as follows. The k th row of the discrete



Figure 13: Possible partitioning of the domain without (left) and with (right) additional partitioning by disconnected component, with each subdomain/component depicted by a color block.

coarse matrix \mathbf{R}_H and therefore the k th column of \mathbf{R}_H^T is given by

$$(\mathbf{R}_H^T)_k = \widehat{\mathbf{R}}_k^T \widehat{\mathbf{D}}_k \widehat{\mathbf{R}}_k \mathbf{1}$$

for $k = 1, \dots, m$, where $\widehat{\mathbf{R}}_k$ and $\widehat{\mathbf{D}}_k$ are the restriction and partition of unity matrices corresponding to $\widehat{\Omega}_k$ and $\mathbf{1}$ is a vector full of ones.

Figure 14 reports convergence histories of the preconditioned GMRES method using the Nicolaides and Trefftz-like coarse spaces for the data set including both walls and buildings. Table 2 summarizes the numerical performance for data sets including or excluding walls. In particular, for both preconditioners, it reports the dimensions of the coarse spaces, as well as the number of GMRES iterations required to achieve a relative L^2 error of 10^{-8} .

As we provide numerical results for various numbers of subdomains N and the computational domain Ω remains fixed independently of N , the results of this experiment should be interpreted in terms of a strong scalability. However, we wish to stress that the fine-scale triangulation is conforming to the nonoverlapping partitioning $(\Omega_j)_{j=1,\dots,N}$. Consequentially, the system (16) changes from one coarse partitioning to another. Nevertheless we ensure that the dimension of the system (16) is roughly constant throughout the experiment for a given N .

The performance of the Trefftz coarse space appears to be very robust with respect to both N and the complexity of the computational domain. While the Nicolaides space is also fairly robust with respect to N (as expected), the Trefftz-like space provides an additional acceleration in terms of iteration count. The improvement with respect to the alternative Nicolaides approach is quite striking,

Table 2: GMRES iterations, dimension, and relative dimension for the Trefftz-like and Nicolaides coarse spaces. Results are shown for minimal geometric overlap and $\frac{1}{20}H$. As the dimension of the Nicolaides space will change with respect to the overlap, its dimension is given as the average dimension over the two overlap values.

		Nicolaides			Trefftz		
		it.		dim. (rel)	it.		dim. (rel)
N		min.	$\frac{H}{20}$		min	$\frac{H}{20}$	
16	no walls	149	51	21 (1.3)	52	28	170 (6.8)
	walls	348	70	96 (6.0)	56	22	400 (16.0)
64	no walls	164	78	85 (1.3)	50	28	433 (5.3)
	walls	359	132	256 (4.0)	56	26	880 (10.9)
256	no walls	136	81	312 (1.2)	56	27	1010 (3.5)
	walls	317	159	719 (2.8)	59	30	1912 (6.6)
1024	no walls	120	83	1204 (1.2)	56	28	2500 (2.3)
	walls	362	174	2044 (2.0)	61	28	4253 (3.9)

especially in the case of the minimal geometric overlap. As expected, increased overlap in the first level of the Schwarz preconditioner provides additional acceleration in terms of iteration count. However, for the Trefftz space, the results with minimal geometric overlap appear to already be quite reasonable.

The dimensions and the relative dimensions of the two coarse spaces are reported in Table 2. Relative dimension refers to the would-be dimension of the coarse space in the case of a domain without perforations with $\Omega_S = \emptyset$; that is, the relative dimensions are computed as $\frac{\dim(R_H)}{(\sqrt{N}+1)^2}$ for the Trefftz space and as $\frac{\dim(R_H)}{N}$ for the Nicolaides space. We observe that the Trefftz space requires a much larger number of degrees of freedom, which naturally leads to a large coarse system to solve. Therefore, the dimension of the Trefftz space is generally larger than Nicolaides, but we note that the contrast between the dimensions of two spaces reduces as N grows. In general, the dimension of the Trefftz-like coarse space appears reasonable given the geometrical complexity of the computational domain.

5. Conclusions

We presented a theoretical and numerical study of the Trefftz coarse space for the Poisson problem posed in domains that include a large number perforations, such as those encountered in the field of urban hydraulics. The main theoretical contribution concerns the error estimate regarding the H^1 -projection over the

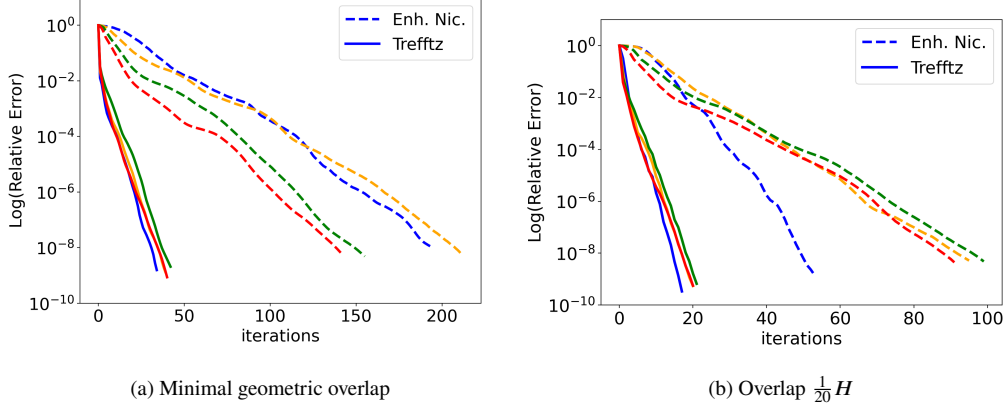


Figure 14: Convergence curves for the Trefftz-like (solid lines) and Nicolaides (dashed lines) coarse spaces for the larger data set involving both buildings and walls and two overlap sizes. Colors correspond to the number of subdomains as follows: $N = 16$ (blue), $N = 64$ (orange), $N = 256$ (green), $N = 1024$ (red).

coarse space. The error analysis does not rely on global regularity of the solution and is performed under some very minimal assumptions regarding the geometry of the domain. In accordance to the presented error analysis, for a specific edge refinement procedure, the coarse approximation achieves superconvergence. This superconvergence is observed in the numerical experiment involving the L-shaped domain. Combined with RAS, the Trefftz space leads to an efficient and robust iterative solver or preconditioner for linear systems resulting from fine-scale finite element discretizations. The performance of the two-level RAS method is demonstrated through numerical experiments involving realistic urban geometries. We observe that, for finite element discretizations with moderate accuracy, the stationary iteration the two-level RAS method reaches the precision of the fine-scale discretization in a few iterations. Used in combination with domain decomposition methods as a preconditioner for Krylov methods, the coarse space provides significant acceleration in terms of Krylov iteration counts when compared to a more standard Nicolaides coarse space. This improvement comes at the price of a somewhat larger coarse problem with a larger dimension. Future work involves extending the presented two-level preconditioning strategy to nonlinear PDEs that model free-surface flows.

Acknowledgments

This work has been supported by ANR Project Top-up (ANR-20-CE46-0005). The high-resolution structural data has been provided by Métropole Nice Côte d’Azur. We warmly thank Florient Largeron, chief of MNCA’s SIG 3D project, for his help in preparation of the data and for the multiple fruitful discussions.

References

- [1] Aarnes, J., Hou, T.Y., 2002. Multiscale domain decomposition methods for elliptic problems with high aspect ratios. *Acta Mathematicae Applicatae Sinica* 18, 63–76.
- [2] Abily, M., Bertrand, N., Delestre, O., Gourbesville, P., Duluc, C.M., 2016. Spatial global sensitivity analysis of high resolution classified topographic data use in 2d urban flood modelling. *Environmental Modelling & Software* 77, 183–195.
- [3] Alonso, R., Santillana, M., Dawson, C., 2008. On the diffusive wave approximation of the shallow water equations. *European Journal of Applied Mathematics* 19, 575–606.
- [4] Andres, L., 2012. L’apport de la donnée topographique pour la modélisation 3D fine et classifiée d’un territoire. *Rev. XYZ* 133, 24–30.
- [5] Araya, R., Harder, C., Paredes, D., Valentin, F., 2013. Multiscale hybrid-mixed method. *SIAM Journal on Numerical Analysis* 51, 3505–3531.
- [6] Arioli, M., Loghin, D., Wathen, A.J., 2005. Stopping criteria for iterations in finite element methods. *Numerische Mathematik* 99, 381–410.
- [7] Babuska, I., Caloz, G., Osborn, J.E., 1994. Special finite element methods for a class of second order elliptic problems with rough coefficients. *SIAM Journal on Numerical Analysis* 31, 945–981.
- [8] Babuska, I., Lipton, R., 2011. Optimal local approximation spaces for generalized finite element methods with application to multiscale problems. *Multiscale Modeling and Simulation* 9, 373–406.
- [9] Boutilier, M., Brenner, K., Dolean, V., 2022. A Trefftz-like coarse space for the two-level Schwarz method on perforated domains. *arXiv preprint arXiv:2211.05880*.

- [10] Boutilier, M., Brenner, K., Dolean, V., 2023. Trefftz approximation space for poisson equation in perforated domains. *Finite Volumes for Complex Applications X—Volume 1, Elliptic and Parabolic Problems* , 195–203.
- [11] Brenner, K., Groza, M., Guichard, C., Lebeau, G., Masson, R., 2016. Gradient discretization of hybrid dimensional darcy flows in fractured porous media. *Numerische Mathematik* 134, 569–609.
- [12] Brezis, H., Mironescu, P., 2018. Gagliardo–nirenberg inequalities and non-inequalities: the full story, in: *Annales de l’Institut Henri Poincaré C, Analyse non linéaire*, Elsevier. pp. 1355–1376.
- [13] Brezzi, F., Falk, R.S., Marini, L.D., 2014. Basic principles of mixed virtual element methods. *ESAIM: Math. Model. Numer. Anal.* 4, 1227–1240.
- [14] Bris, C.L., Legoll, F., Madiot, F., 2019. Multiscale finite element methods for advection-dominated problems in perforated domains. *Multiscale Modeling & Simulation* 17, 773–825.
- [15] Casulli, V., 1990. Semi-implicit finite difference methods for the two-dimensional shallow water equations. *Journal of Computational Physics* 86, 56–74.
- [16] Degond, P., Lozinski, A., Muljadi, B.P., Narski, J., 2015. Crouzeix-raviart msfem with bubble functions for diffusion and advection-diffusion in perforated media. *Communications in Computational Physics* 17, 887–907.
- [17] Dohrmann, C.R., Klawonn, A., Widlund, O.B., 2008. Domain decomposition for less regular subdomains: Overlapping Schwarz in two dimensions. *SIAM Journal on Numerical Analysis* 46, 2153–2168.
- [18] Dolean, V., Nataf, F., Scheichl, R., Spillane, N., 2012. Analysis of a two-level schwarz method with coarse spaces based on local dirichlet-to-neumann maps. *Computational Methods in Applied Mathematics* 12, 391–414.
- [19] Dryja, M., Sarkis, M.V., Widlund, O.B., 1996. Multilevel schwarz methods for elliptic problems with discontinuous coefficients in three dimensions. *Numerische Mathematik* 72, 313–348.
- [20] Dryja, M., Smith, B.F., Widlund, O.B., 1994. Schwarz analysis of iterative substructuring algorithms for elliptic problems in three dimensions. *SIAM Journal on Numerical Analysis* 31, 1662–1694.

- [21] Ern, A., Guermond, J.L., Ern, A., Guermond, J.L., 2004. Finite element interpolation. *Theory and Practice of Finite Elements* , 3–80.
- [22] Galvis, J., Efendiev, Y., 2010. Domain decomposition preconditioners for multiscale flows in high-contrast media. *Multiscale Modeling and Simulation* 8, 1461–1483.
- [23] Gander, M.J., Loneland, A., Rahman, T., 2015. Analysis of a new harmonically enriched multiscale coarse space for domain decomposition methods. *arXiv preprint arXiv:1512.05285* .
- [24] Graham, I.G., Lechner, P., Scheichl, R., 2007. Domain decomposition for multiscale PDEs. *Numerische Mathematik* 106, 589–626.
- [25] Hajibeygi, H., Bonfigli, G., Hesse, M.A., Jenny, P., 2008. Iterative multiscale finite-volume method. *Journal of Computational Physics* 19, 8604–8621.
- [26] Heinlein, A., Klawonn, A., Knepper, J., Rheinbach, O., 2018. An adaptive GDSW coarse space for two-level overlapping Schwarz methods in two dimensions, in: *Domain Decomposition Methods in Science and Engineering XXIV* 24, pp. 373–382.
- [27] Hou, T.Y., Wu, X.H., 1997. A multiscale finite element method for elliptic problems in composite materials and porous media. *Journal of Computational Physics* 134, 169–189.
- [28] Jiránek, P., Strakovs, Z., Vohralík, M., 2010. A posteriori error estimates including algebraic error and stopping criteria for iterative solvers. *SIAM Journal on Scientific Computing* 32, 1567–1590.
- [29] Le Bris, C., Legoll, F., Lozinski, A., 2014. An MsFEM type approach for perforated domains. *Multiscale Modeling & Simulation* 12, 1046–1077.
- [30] Ma, C., Scheichl, R., Dodwell, T., 2022. Novel design and analysis of generalized finite element methods based on locally optimal spectral approximations. *SIAM Journal on Numerical Analysis* 60, 244–273.
- [31] Målqvist, A., Peterseim, D., 2014. Localization of elliptic multiscale problems. *Mathematics of Computation* 83, 2583–2603.

- [32] Mandel, J., Brezina, M., 1996. Balancing domain decomposition for problems with large jumps in coefficients. *Mathematics of Computation* 65, 1387–1401.
- [33] Nataf, F., Xiang, H., Dolean, V., Spillane, N., 2011. A coarse space construction based on local Dirichlet-to-Neumann maps. *SIAM Journal on Scientific Computing* 33, 1623–1642.
- [34] Nicolaides, R.A., 1987. Deflation of conjugate gradients with applications to boundary value problems. *SIAM Journal on Numerical Analysis* 24, 355–365.
- [35] Rudin, W., et al., 1973. *Functional analysis*. New York: McGraw-Hill,.
- [36] Scheichl, R., Vassilevski, P.S., Zikatanov, L.T., 2012. Multilevel methods for elliptic problems with highly varying coefficients on nonaligned coarse grids. *SIAM Journal on Numerical Analysis* 50, 1675–1694.
- [37] Shewchuk, J.R., 1996. Triangle: Engineering a 2d quality mesh generator and delaunay triangulator, in: *Workshop on applied computational geometry*, Springer. pp. 203–222.
- [38] Spillane, N., Dolean, V., Hauret, P., Nataf, F., Pechstein, C., Scheichl, R., 2014. Abstract robust coarse spaces for systems of PDEs via generalized eigenproblems in the overlaps. *Numerische Mathematik* 126, 741–770.
- [39] Taralova, V., 2015. Upscaling approaches for nonlinear processes in lithium-ion batteries. Ph.D. thesis. Technische Universität Kaiserslautern.
- [40] Beir ao da Veiga, L., Chernov, A., Mascotto, L., Russo, A., 2016. Basic principles of hp virtual elements on quasiuniform meshes. *Mathematical Models and Methods in Applied Sciences* 26, 1567–1598.
- [41] Weinan, E., Engquist, B., 2003. The heterogeneous multiscale methods. *Communications in Mathematical Sciences* 1, 87–132.
- [42] Weißer, S., 2019. *BEM-based Finite Element Approaches on Polytopal Meshes*. volume 130. Springer.
- [43] Yu, D., Lane, S.N., 2006a. Urban fluvial flood modelling using a two-dimensional diffusion-wave treatment, part 1: mesh resolution effects. *Hydrological Processes: An International Journal* 20, 1541–1565.

- [44] Yu, D., Lane, S.N., 2006b. Urban fluvial flood modelling using a two-dimensional diffusion-wave treatment, part 2: development of a sub-grid-scale treatment. *Hydrological Processes: An International Journal* 20, 1567–1583.